Chemically deposited magnesium hydroxide thin film

P. S. Das[†1], A. Dey[†1,2], M. R. Chaudhuri[1], S. Roy[1], N. Dey[1], A. K. Mandal[1] and A. K. Mukhopadhyay*[1]

Here we report for the first time to the best of our knowledge the processing techniques, nucleation kinetics and the nanoindentation behaviour of a 1·5 μm magnesium hydroxide thin film chemically deposited on a commercially available soda lime silica glass substrate at room temperature. The phase and microstructure of the films were analysed by X-ray diffraction, scanning electron microscopy, field emission scanning electron microscopy as well as transmission electron microscopy. An exponential nucleation kinetics was identified for the growth of the thin films. The nanomechanical properties, e.g. nanohardness and Young's modulus of the films were measured by the nanoindentation technique at ultralow loads of 50, 70 and 100 μN. Finally, the nature of deformation of the thin film was analysed in terms of the energetics of the nanoindentation process and the microstructure.

Keywords: Magnesium, Hydroxide, Film, Nucleation, Nanoindentation, Energy

Introduction

Nowadays, thin films are considered as a highly promising material for biomedical, energy, optical, sensing related applications[1–4] as well as for corrosion protection of magnesium alloys.[5–8] In this regard, magnesium oxide is a very important protective material that can be *in situ* formed from the magnesium hydroxide [$Mg(OH)_2$] thin film[9] precursors. The most recently emerging application of magnesium hydroxide is as a buffer layer for the copper indium gallium selenium[10] and dye sensitised solar cells.[11] Most recently reported methods for preparation of magnesium hydroxide include hydrothermal synthesis,[12] precipitation[13] and surfactant mediated solution.[14] The hydrothermal method[12] requires autoclaving under stringent temperature and pressure control thereby making it comparatively more energy and cost intensive. The wet precipitation method,[13] although simple to handle, requires the use of dispersant and does not provide the formation of a coating on a given substrate as it precipitates only the nanoparticles of $Mg(OH)_2$. Similarly, the method of surfactant mediation[14] requires stringent control of interface chemistry and yet provides only ordered array of $Mg(OH)_2$ nanoparticles and not a coating on a given substrate.

However, the chemical deposition process[10] has many distinct advantages over the aforementioned processes. First of all, it can be used for deposition over a relatively larger area. Second, the process can be fully automated by relatively simpler means. Third, the process involves simple chemical principles that can be handled with relative ease. In fact, the process can even be exploited for fabrication of low cost solar cells.[10] Another great advantage of this process is that it is flexible. Thus, if needed, changes can be incorporated in the chemical bath composition without much hazard. Finally, a huge capital cost is usually not involved in the chemical deposition process. By controlling the pH of the corresponding solutions and the dipping time as well as the number of dipping, the microstructure, thickness and hence the physical/chemical properties of the thin films can be easily fine tuned. Furthermore, for solar cell applications, the films of the buffer layer will need to have a thickness, e.g. $\leqslant$1–2 μm similar to those of the CIGS thin films themselves.[10] This can be more easily achieved by chemical deposition in a manner that is less cost intensive. The thickness compatibility is required to ensure lesser recombination at the interface so that a beneficial effect occurs in terms of the efficiency of the solar cells.[10,11]

On the other hand, the nanoindentation technique has recently[15–17] emerged as a very important technique for characterisation of nanomechanical properties of thin films and coatings. In spite of the wealth of literature,[9–14] there has not been any systematic study of the nucleation kinetics as well as the nanomechanical properties of chemically deposited magnesium hydroxide thin films. Therefore, the objective of the present work was to evaluate the nucleation kinetics and the nanomechanical properties of chemically deposited $Mg(OH)_2$ thin films on soda lime silica (SLS) glass substrates.

[†] These authors contributed equally to this research work.

[1]CSIR – Central Glass and Ceramic Research Institute, Kolkata 700 032, India
[2]Present address: Thermal Systems Group, ISRO Satellite Centre, Vimanapura, Post, Bangalore 560017, India

*Corresponding author, email anoopmukherjee@cgcri.res.in

Published by Maney on behalf of the Institute
Received 9 March 2012; accepted 2 August 2012
DOI 10.1179/1743294412Y.0000000055

Materials and methods

Magnesium hydroxide thin films were deposited onto precleaned and dried commercially available SLS glass slides ($25 \times 25 \times 1{\cdot}15$ mm) by the conventional chemical deposition method from 0·1M aqueous solutions of magnesium nitrate, $Mg(NO_3)_2$ (reagent grade; Ranbaxy, Mumbai, India) and sodium hydroxide, NaOH (reagent grade; Qualigens Fine Chemicals, Kolkata, India) using the following chemical reaction at room temperature

$$Mg(NO_3)_2 + 2NaOH = Mg(OH)_2 + 2NaNO_3 \quad (1)$$

For this purpose, 4·36 g L^{-1} aqueous sodium hydroxide (NaOH, MW=40·0) and 25·84 g L^{-1} aqueous magnesium nitrate [$Mg(NO3)_2.6H_2O$, MW=256·43] solutions were prepared using double distilled water. Each of the above solutions of 100 mL were taken into two separate beakers. The pH values of sodium hydroxide and magnesium nitrate solutions were ~12 and 6·8 respectively. The substrates were sequentially dipped vertically first into magnesium nitrate and then into sodium hydroxide solutions by a programmable dip coater machine at a suitable uniform rate of ~1 mm min^{-1}. The process was repeated several times to affect the nucleation and growth of the magnesium hydroxide film and the total time for the requisite number of dipping were calculated. The film on glass slide surface was washed several times very carefully with double distilled water. Then the films were dried at room temperature and finally for 30 min at 100–110°C in a hot air oven. From the difference of the weights of the substrate with and without the film in a chemical balance with an accuracy of 10^{-4} g, the actual weight of the deposited film was determined for a given experimental condition. After final processing, the samples were kept in a vacuum dessiccator at room temperature.

The film thickness was measured by a profilometer (Form Talysurf 120; Taylor Hobson, UK). The phase purity was evaluated by X-ray diffraction (XRD; monochromatic Cu $K_{\alpha 1}$ radiation, 35 mA, 40 kV; X'pert Pro MPD diffractometer; PANalytical, The Netherlands). Surface morphology of the coating was characterised by scanning electron microscopy (SEM; s430i; Leo, UK), field emission scanning electron microscopy (FE-SEM; Supra VP35; Carl Zeiss, Germany) and transmission electron microscopy (TEM; Tecnai G^2 30, S-Twin, 300 kV; FEI, The Netherlands; LaB_6 filament, line resolution 0·14 nm and point resolution 0·2 nm). To avoid charging, a 50–70 nm carbon coating was deposited on the $Mg(OH)_2$ thin film by the arc deposition technique before insertion in the sample chamber for SEM. Before TEM observation, the sample was deposited onto Cu grids, supported with a carbon film. The samples were deposited onto the support grids by deposition from a dilute suspension in acetone.

The nanoindentation experiments[18–20] were conducted with a commercial nanoindenter (TriboIndenter Ubi 700; Hysitron Inc., Minneapolis, USA). The details of the experimental procedures have been given elsewhere[18] and hence, will be only briefly mentioned here. The nanohardness and Young's modulus data of the present $Mg(OH)_2$ thin films were calculated from the load P versus depth of penetration h data of the aforesaid nanoindentation experiments by using Oliver and Pharr[19] method. The machine gave the reduced Young's moduli data of the $Mg(OH)_2$ thin films. These data were used to calculate the Young's moduli data of the present $Mg(OH)_2$ thin films following the method given in Ref. 19 assuming a Poisson's ratio value of 0·25, typical of ceramics[19] because no experimental data on Possion's ratio of $Mg(OH)_2$ thin films were available in literature.

The machine had a load resolution of 1 nN along z axis while the depth resolution was 0·04 nm along z axis. Furthermore, the thermal drift was maintained at $<0{\cdot}05$ nm s^{-1}. All the nanoindentation experiments whose results are reported in the present work were conducted at room temperature (~30°C) and ~70% relative humidity. The machine provided a P–h plot in nanoindentation mode using a tetrahedral diamond Berkovich tip of ~150 nm tip radius and semi-apex angle ~65·3°. The diamond Berkovich tip had a Poisson's ratio of 0·07 and a Young's modulus of 1140 GPa.[20] In all the experiments, a constant loading rate of 10 μN s^{-1} was used. The unloading rate was the same as the loading rate. The dwell time at peak load was 0 s. As soon as the peak load was reached, the sample was unloaded at the given unloading rate instantly and the loading and unloading P–h data were automatically recorded by the machine.

At least 16 nanoindents (i.e. 4×4 array) were made at each of the five randomly chosen different locations of the sample. Thus, each reported value of nanohardness was an average of at least 80 or more individual data points. In addition, the unloading part of the experimental P–h plot was analysed according to the Oliver–Pharr model[19] following the equation

$$P = \alpha(h - h_f)^m \quad (2)$$

where h is the instantaneous depth of penetration at a nanoindentation load P, h_f is the final depth of penetration, and α and m are fitting parameters.

For conducting the nanoindentation experiments, the $Mg(OH)_2$ thin films were mounted on a motorised table that allowed for a movement in the plane normal to the axial motion of the tip. The transducer that measured both load and depth consisted of a three-plate capacitor. It had the same tetrahedral diamond Berkovich tip of ~150 nm tip radius as mentioned above, attached to its central plate. The instrument was calibrated before each and every experiment by performing indents of increasing depth in a standard fused quartz sample provided by the supplier of the machine. The standard fused quartz sample had a known[18] nanohardness of $9{\cdot}25 \pm 0{\cdot}93$ GPa and a reduced Young's modulus E_r of $69{\cdot}6 \pm 3{\cdot}48$ GPa. In the present experiments, three different peak loads, e.g. 50, 70 and 100 μN were applied.

Results and discussion

The thickness of the $Mg(OH)_2$ film was measured as ~1·5 μm. The phase purity of the synthesised thin films was confirmed by the typical XRD data (Fig. 1*a*; JCPDS file no: 7–239). The crystallite sizes estimated by the Scherer's method[21,22] were 1·75, 4·77, 3·70, 9·34, 5·99, 2·89, 5·57 and 4·26 nm corresponding to the broadened peaks (001), (101), (102), (110), (111), (103), (201) and (202) respectively. Corresponding to the strongest peak (101), the lattice parameters were calculated as $a=b=3{\cdot}1449$ Å and $c=4{\cdot}78500$ Å which matched well with reported data.[21]

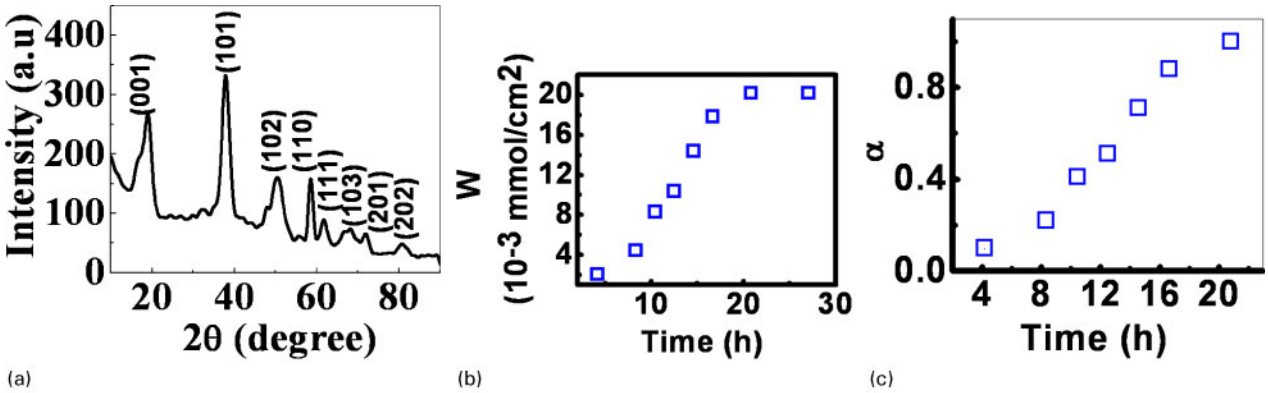

1 ***a*** **XRD spectra of $Mg(OH)_2$ thin film,** ***b*** **amount of Mg^{2+} ions and** ***c*** **α as function of time for deposition of $Mg(OH)_2$ thin film**

Figure 1*b* shows that the amount of Mg^{+2} ions W (mmol cm^{-2}) increased slowly with time up to about 10 h and abruptly after ~10·45 h before becoming nearly constant beyond ~20·83 h; whereby with a sluggish growth rate, the final dried film thickness of 1·5 μm is reached after ~27·08 h. This result suggested that the equilibrium between film formation and dissolution had happened during the present chemical deposition process.

Figure 1*c* shows the data on the extent of reduced reaction α for Mg^{+2} ions versus time where α (Ref. 23) represents the fraction of Mg^{+2} ions that can be obtained after a given time t divided by the equilibrium amount of Mg^{+2} ions in the film. The value of α varies from 0 at the beginning of the reaction to 1 at equilibrium reached after ~21 h (Fig. 1*b*). The data are best fitted by the expression: $\alpha = 0{\cdot}0105t^{1{\cdot}5368}$ with a correlation coefficient R^2 of ~0·98. Following Ref. 23, simple algebraic manipulation leads to the nucleation kinetics equation: $d\alpha/dt \approx 0{\cdot}38\alpha^{0{\cdot}4}$ that approximately resembles the Maple equation for exponential nucleation.

The cross-sectional SEM (Fig. 2*a*) confirmed that film had a relatively dense microstructure although there was apparently some residual porosity. The FE-SEM photomicrograph gave evidence that the film had a layered platelet like architecture comprising of the $Mg(OH)_2$ nanocrystallites (Fig. 2*b*). The nanocrystallites appeared from the FE-SEM photomicrograph to have formed the platelets (Fig. 2*c*) in a given layer. Further, such layers appeared from the FE-SEM photomicrograph to be stacked upon one another with a typical inter layer distance of about 10-30 nm (Fig. 2*d*).

The TEM photograph confirmed that the platelets had a hexagonal shape (Fig. 3*a*). Their size had a Gaussian distribution with an average of about $108{\cdot}04 \pm 23{\cdot}53$ nm (Fig. 3*b*) and a selected area electron diffraction pattern typical of thin films (inset, Fig. 3*a*).

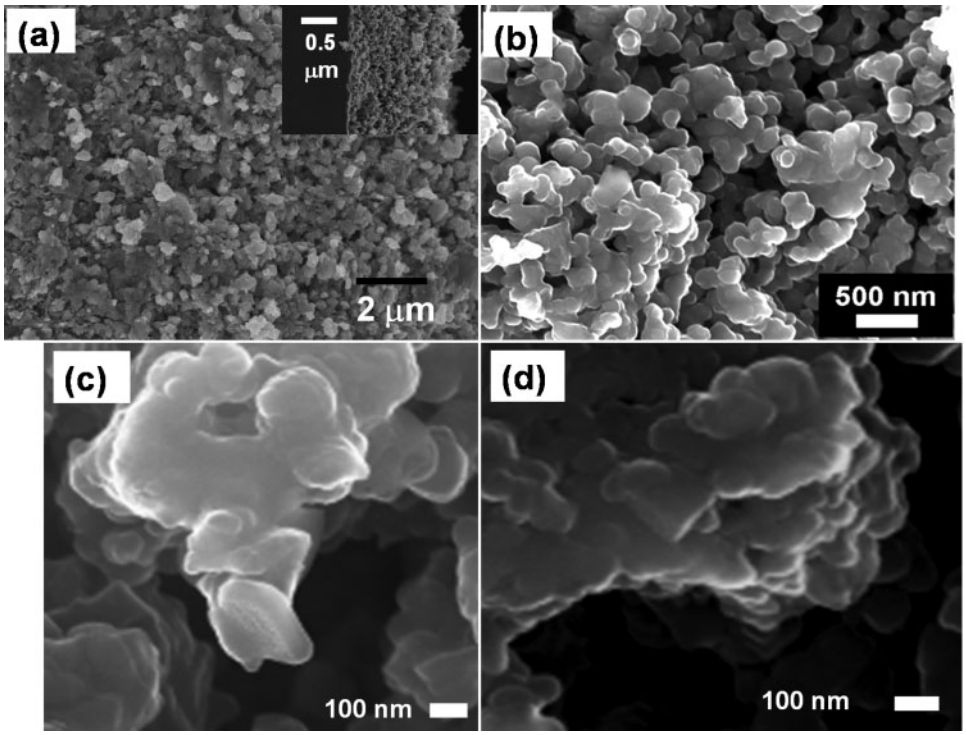

2 Microstructure of $Mg(OH)_2$ thin film: ***a*** **cross-sectional SEM showing realatively dense microstructure (inset shows film on glass substrate); FE-SEM images showing** ***b*** **a layered platelet type architecture,** ***c*** **nanocrystallites forming platelets and** ***d*** **stacking of layers**

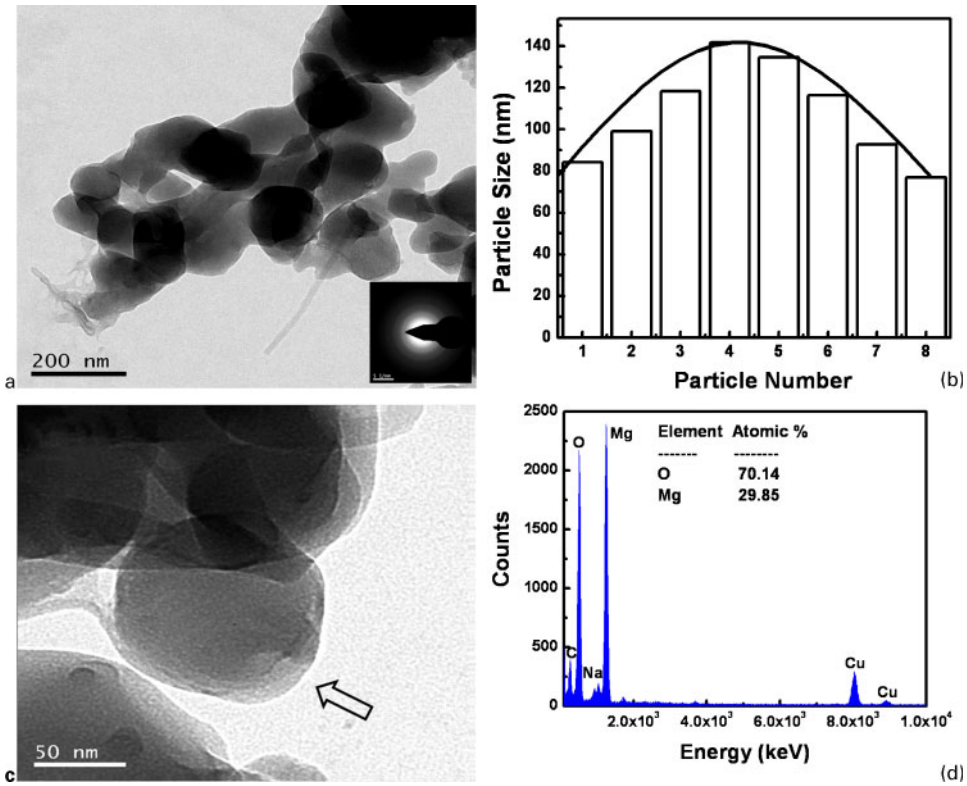

3 Images (TEM) of $Mg(OH)_2$ thin film showing *a* platelet structure of nanocrytallites that formed layered structure (inset: typical selected area electron diffraction pattern), *b* Gaussian size distribution of platelets, *c* single platelet and *d* energy dispersive X-ray data of film

The average size of the platelets as obtained from the Gaussian distribution tallies with the typical size (107·17 nm) of a single platelet (Fig. 3*c*). The platelet composed of a large number of about 1–10 nm size nanocrystallites. The average size of such a range matched favourably with the average (4·79 ± 2·30 nm) of those estimated from the XRD data (Fig. 1*a*). It had a thickness of ~15·6 nm. In terms of order of

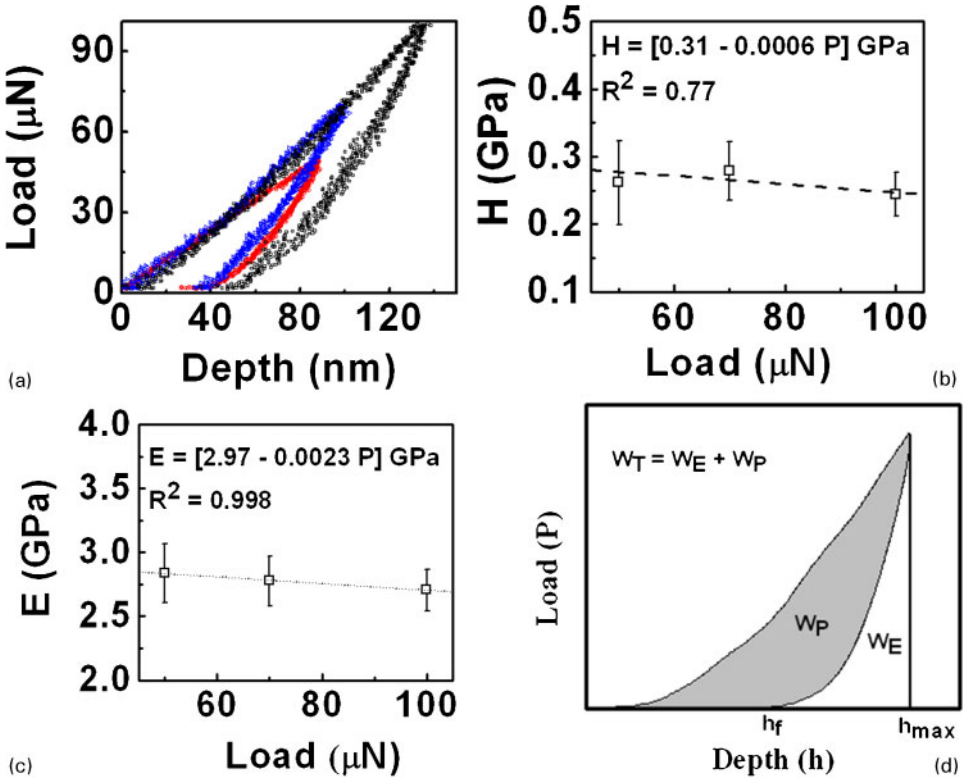

4 Nanoindentation data of $Mg(OH)_2$ thin film *a* typical load depth plots, *b* nanohardness, *c* Young's moduli and *d* schematic of elastic and plastic energy spent in nanoindentation experiments

magnitude, these data also tally with the average of the typical inter layer distance of about 10–30 nm as observed from FE-SEM image (Fig. 2*d*).

This picture also matches with the fact that the crystal structure of $Mg(OH)_2$ is a layered CdI2 type arrangement. It comprises of successive hexagonal Mg^{2+} ion layers and OH^- ion layers stacked one upon each other. The sixfold coordination of the magnesium cation by hydroxyl groups forms a $Mg(OH)_6^{-4}$ octahedron.[24,25]

Typical energy dispersive X-ray data showed ~29·85 at-%Mg and ~70·14 at-%O (Fig. 3*d*), suggesting that the present films were somewhat rich in oxygen content and lean in magnesium content compared with those of an ideal defect free material.[26] The peak for carbon came from the carbon coating and that of copper from the copper grid used to hold the sample.

For nanoindentation loads P of 50, 70 and 100 μN, the maximum depths of penetrations were ~90, 100 and 140 nm which were well below 10% of film thickness (1·5 μm) (Fig. 4*a*). The average elastic recovery[19] was ~70%.

The nanohardness and Young's moduli of the $Mg(OH)_2$ thin films were $0{\cdot}26\pm0{\cdot}06$, $0{\cdot}28\pm0{\cdot}04$ and $0{\cdot}24\pm0{\cdot}03$ GPa (Fig. 4*b*) and $2{\cdot}83\pm0{\cdot}23$, $2{\cdot}77\pm0{\cdot}19$ and $2{\cdot}70\pm0{\cdot}16$ GPa (Fig. 4*c*) respectively at loads of 50, 70 and 100 μN. The best fit equations given as insets of Fig. 4*a* and *b* respectively, predicted nanohardness of 0·31 GPa and Young's modulus of 2·97 GPa.

To the best of our knowledge, this is the first experimental data on nanohardness and Young's modulus of chemically deposited $Mg(OH)_2$ thin films on SLS glass substrates. There is unfortunately no other published data on the nanomechanical properties of magenesium hydroxide either in thin film or in bulk form either. So, a direct comparison of the data from the present work with those from literature was not possible. However, from the reported data for exfoliated CoAl layered double hydroxide/polyamide 6 nanocomposites by *in situ* polymerisation,[27] the nanohardness and Young's modulus of a CoAl layered double hydroxide were evaluated by the rule of mixtures to be ~0·34 and 7·73 GPa which compared favourably with the present data of 0·31 and 3 GPa for nanohardness and Young's modulus respectively. There was no particular reason or bias for choosing this particular material's data except that to the best of our knowledge it was the only one data on nanomechanical properties of layered double hydroxide available in literature.

The amounts of energy spent in plastic, i.e. irrecoverable deformation, elastic, i.e. recoverable deformation and their sum total during the nanoindentation experiments are termed[19] as W_P, W_E and W_T respectively. This aspect is schematically indicated in Fig. 4*d*. The grey shaded part in Fig. 4*d* represents the energy spent in plastic deformation, i.e. W_P. The white shaded part in Fig. 4*d* represents the energy spent in plastic deformation, i.e. W_E. The total area under the load–displacement plot represents the total amount of energy spent in deformation, i.e. $W_T = W_E + W_P$. In the present $Mg(OH)_2$ thin films chemically deposited on SLS glass substrates, depending on the peak load, the ratio W_P/W_T varied in the range from ~0·57 to 0·43 while the ratio W_E/W_T varied in a complimentary fashion in the range from ~0·43 to 0·57 (Fig. 5), assuming that $W_T = W_E + W_P$.[19]

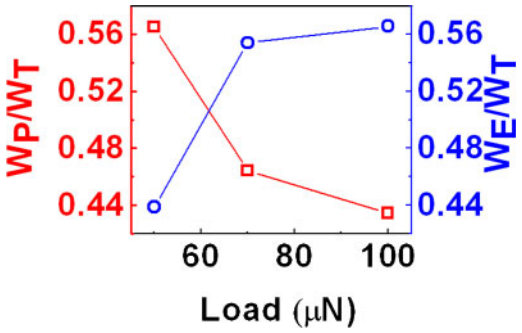

5 Energy ratio as function of load applied in nanoindentation experiments on $Mg(OH)_2$ thin films

The present data (Fig. 5) matched well with reported experimental data[28] on other materials. The decreasing trend of W_P/W_T (Fig. 5) with the increase in load happened because the ratio h_f/h_{max} (Ref. 19) decreased from ~31% at 50 μN load to ~28% at 100 μN load (Fig. 4*a*). Here, h_f has been already defined and h_{max} refers to the maximum depth of penetration for a given peak load attained during the nanoindentation experiments. These data implies that at 50 μN load, ~69% of the maximum penetration depth was elastically recovered while at 100 μN load ~72% of the same was elastically recovered. Thus, the increasing trend of W_E/W_T with the increase in nanoindentation load (Fig. 5) possibly reflected the fact that the current $Mg(OH)_2$ thin films had a microstructure that was inherently capable of more elastic recovery the more it is deformed. It is suggested that the layered microstructure of the chemically deposited magnesium hydroxide thin films helped to accommodate the strain due to the applied nanoindentation load and thereby affect the elastic recovery through localised rearrangements on withdrawal of the nanoindenter during the unloading cycle.

Fitting the data from unloading part of the nanoindentation load versus depth plots (Fig. 4*a*) to the equation (1) gave 'α'of about 0·017–0·024 (Fig. 6) which matched with experimental data reported for other materials[19] and 'm' of about 1·79–1·92 with an average of $1{\cdot}86\pm0{\cdot}06$ which suggested the conical punch geometry as the best approximation for the present nanoindenter following Sneddon's analysis.[29]

Finally, it should be mentioned that depending on load, the nanohardness of the $Mg(OH)_2$ thin films was about 0·24–0·28 GPa. It is evident from Figs. 2 and 3 that the present film was not fully dense and it appeared to have some amount of residual porosity as mentioned earlier although an exact estimation of the same was beyond the scope of the present work. The presence of porosity in the film can degrade the nanohardness as it has been reported[30] that the same of microplasma sprayed hydroxyapatite coatings could be much lower than those of their dense, bulk counterparts due to presence of about 10–20 vol.-% open porosity. A similar statement is true for the Young's moduli data of the present $Mg(OH)_2$ thin films chemically deposited on SLS glass substrates because it has been demonstrated[31] already that the presence of larger volume per cent porosity decreases the load bearing contact area and thereby the Young's modulus.

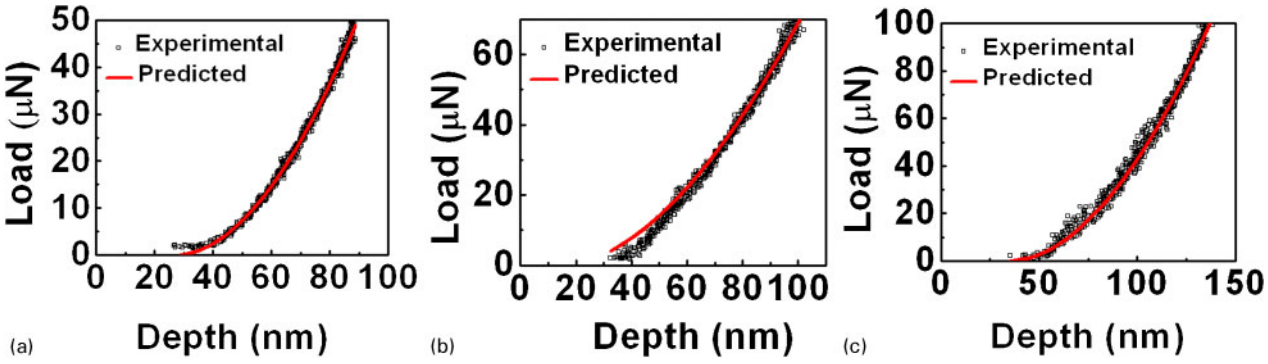

6 Fitting of unloading data from Fig. 4*a* to equation (1) at different peak loads (hollow symbols: experimental data; solid lines: predicted trend): *a* 50 μN; *b* 70 μN; *c* 100 μN

Conclusion

A simple, inexpensive chemical deposition technique produced a 1·5 μm nanostructred pure magnesium hydroxide film with an exponential nucleation kinetics on SLS glass substrates. By virtue of a strain tolerant layered microstructure the films showed nanohardness ~0·3 GPa and Young's modulus ~3 GPa. Thus, the nanostructured pure magnesium hydroxide film may be useful for protective as well as functional applications.

Acknowledgements

The kind permission of Director, CGCRI to publish this paper, the infrastructural supports received from the XRD and electron microscopy sections as well as the financial support of CSIR (project no. NWP 0027) are gratefully acknowledged.

References

1. B. Čolović, B. Todorović-Marković, Z. Marković, D. Marković, M. Plavšić and V. Jokanović: *Surf. Eng.*, 2010, **26**, 532–535.
2. A. L. Shaula, J. C. Oliveira, A. V. Kolotygin, V. V. Kharton and A. A. Cavaleiro: *Surf. Eng.*, 2010, **26**, 584–589.
3. K. Ravichandran, K. Saravanakumar, G. Muruganantham and B. Sakthivel: *Surf. Eng.*, 2010, **26**, 620–622.
4. C. B. da Silveira, A. F. de Oliveira, S. D. de Campos, A. E. de Campos and A. D. Fraporti: *Surf. Eng.*, 2012, **28**, 68–72.
5. P. S. Bala, C. Blawert, M. Störmer and W. Dietzel: *Surf. Eng.*, 2010, **26**, 340–346.
6. P. S. Bala, N. Scharnagl, C. Blawert and W. Dietzel: *Surf. Eng.*, 2010, **26**, 354–360.
7. P. S. Bala, J. Liang, C. Blawert, M. Störmer and W. Dietzel: *Surf. Eng.*, 2010, **26**, 367–370.
8. H. Wang, Z. H. Chen and L. L. Li: *Surf. Eng.*, 2010, **26**, 385–391.
9. Q. Mao, L. Zhang, D. Huang, D. Wang, Y. Huang, H. Xu, H. Cao and Z. Mao: *Surf. Interface Anal.*, 2012, **43**, 903–912.
10. C.-H. Huang, Y.-L. Jan and W.-C. Lee: *J. Electrochem. Soc.*, 2011, **158**, H879–H888.
11. J. H. Yum, S. Nakade, D. Y. Kim and S. Yamagida: *J. Phys. Chem. B*, 2006, **110B**, 3215–3219.
12. Y. Zhu, Q. Zhao, Y.-H. Zhang and G. Wu: *Surf. Coat. Technol.*, 2012, **206**, 2961–2966.
13. P. Wang, C. Li, H. Gong, H. Wang and J. Liu: *Ceram. Int.*, 2011, **37**, 3365–3370.
14. D. An, X. Ding, Z. Wang and Y. Liu: *Colloid. Surf. A: Physicochem. Eng. Aspect.*, 2010, **356**, 28–31.
15. A. K. Keshri, S. R. Bakshi, Y. Chen, T. Laha, X. Li, C. Levy and A. Agarwal: *Surf. Eng.*, 2009, **25**, 270–275.
16. B. C. Ray: *Surf. Eng.*, 2011, **27**, 551–556.
17. A. K. Prasad, R. Jha, R. Ramaseshan, S. Dash, I. Manna and A. K. Tyagi: *Surf. Eng.*, 2011, **27**, 350–354.
18. A. Dey, R. Chakraborty and A. K. Mukhopadhyay: *Int. J. Appl. Glass Sci.*, 2011, **2**, 144–155.
19. W. C. Oliver and G. M. Pharr: *J. Mater. Res.*, 1992, **7**, 1564–1583.
20. C. E. Packard and C. A. Schuh: *Acta Mater.*, 2007, **55**, 5348–5358.
21. J. C. Yu, A. Xu, L. Zhang, R. Song and L. Wu: *J. Phys. Chem. B*, 2004, **108B**, 64–70.
22. X. Li, D. Diao and B. Bhushan: *Acta Mater.*, 1997, **45**, 4453–4461.
23. Z. Liu, F. Zhang, X. Lei, L. Yang, D. G. Evans and X. Duan: *Chem. Eng. Sci.*, 2007, **62**, 6069–6075.
24. H. R. Oswald, R. Asper and R. M. A. Lieth (eds.): 'Bivalent metal hydroxides in physics and chemistry of mineral with layered structures', Vol. 1, 71; 1977, Dordrecht, Reidel.
25. C. Henrist, J. P. Mathieu, C. Vogels, A. Rulmont and R. J. Cloots: *J. Cryst. Growth*, 2003, **249**, 321–330.
26. H. Sato, A. Morita, K. Ono, H. Nakano, N. Wakabayashi and A. Yamagishi: *Langmuir*, 2003, **19**, 7120–7126.
27. H. Peng, W. C. Tjiu, L. Shen, S. Huang, C. He and T. Liu: *Compos. Sci. Technol.*, 2009, **69**, 991–996.
28. M. T. Ataf: *Mater. Lett.*, 2003, **57**, 4684–4693.
29. I. N. Sneddon: *Int. J. Eng. Sci.*, 1965, **3**, 47–57.
30. A. Dey and A. K. Mukhopadhyay: *Adv. Appl. Ceram.*, 2010, **109**, 346–354.
31. A. K. Mukhopadhyay and K. K. Phani: *J. Eur. Ceram. Soc.*, 2000, **20**, 29–38.